

Learning Crisp Boundaries Using Deep Refinement Network and Adaptive Weighting Loss

Yi-Jun Cao, Chuan Lin, and Yong-Jie Li, *Senior Member, IEEE*

Abstract—Significant progress has been made in boundary detection with the help of convolutional neural networks (CNNs). Recent boundary detection models not only focus on the real object boundary detection but also “crisp” boundaries (precisely localized along the object’s contour). There are two methods to evaluate crisp boundary performance. One uses more strict tolerance to measure the distance between ground truth and the detected contour. The other focuses on evaluating the contour map without any postprocessing. In this paper, we analyze both methods and conclude that both methods are two aspects of crisp contour evaluation. Accordingly, we propose a novel network called deep refinement network (DRNet) that aims at stacking multiple refinement modules to achieve richer feature representation and a novel loss, which combines cross-entropy and dice loss through effective adaptive fusion. Using a pretrained VGG16 network, we achieve state-of-the-art performance on several available datasets.

Index Terms—Contour detection, Decode Network, Deep Refinement Network, Multi-Scale Integration

1 INTRODUCTION

Boundary detection plays a fundamental role in image and video processing applications such as local surface descriptor [1] and image retrieval [2, 3]. In these applications, boundary detection is usually considered a low-level technique and normally used as a shape or boundary constraint to help high-level image tasks to improve their performance.

In the past few years, convolutional neural networks (CNNs) had become popular in the computer vision field and have helped substantially improve many tasks, including image classification [4, 5], object detection [6], and semantic segmentation [7]. Depending on the strong capability of CNNs, contour detection exploits CNNs architectures for higher performance. Many well-known CNN-based methods such as DeepContour [8], HED [9], RCF [10], and CED [11] take remarkable improvement of state-of-the-art F-score on benchmarks such as BSDS500 [12] and NYUDv2 [13].

Although some state-of-the-art methods achieved human-like performance on standard datasets such as BSDS500 [12],

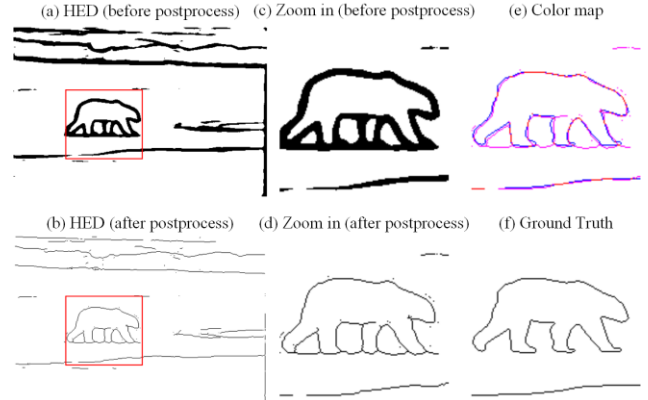


Fig. 1. Visualization of edge maps from HED with and without postprocessing. (a) and (b) show the HED result before and after postprocessing (NMS and morphological thinning, respectively) with a fixed threshold of $t = 0.5$. (c) and (d) show the corresponding zoomed images. (e) shows the color map which the red, blue and purple pixels indicating $E_{GT} \cap E_a \cap E_b$, $E_{GT} \cap D_a \cap E_b$, and $D_{GT} \cap E_a \cap E_b$, respectively, where E and D indicate the contour and background union, respectively; subscript GT , a , and b indicate ground truth, and HED output after and before postprocessing, respectively. (f) shows the Ground Truth.

contour detection is still a challenging problem for extracting more detailed edges. The main reason is that CNN-based methods are highly “correct” yet less “crisp”, i.e., edges are not well localized [11]. As shown in Fig. 1(e), the red and blue pixels indicate $E_{GT} \cap E_a \cap E_b$, $E_{GT} \cap D_a \cap E_b$ with a large tolerance, where E indicate the contour union; subscript GT , a , and b indicate ground truth, HED output after and before postprocessing, respectively. We can observe that the “correct” contour (blue edges) is adequate to describe objects but not enough “crisp” (red edges). This issue is deeply rooted in modern CNN architecture [4] because pooling layers lead to blurred output of edges and a fully convolutional architecture encourages similar responses of neighboring pixels, thus failing to produce a thin edge map. More than just contour detection, semantic segmentation and target detection tasks are also focused on solving fine positioning problems.

This work was supported by the National Natural Science Foundation of China (Grant No. 61866002), Guangxi Natural Science Foundation (Grant No. 2018GXNSFAA138122 and Grant No. 2015GXNSFAA139293), Innovation Project of Guangxi Graduate Education (Grant No. YCSW2018203).

Yi-Jun Cao and Chuan Lin are with the College of Electric and Information Engineering, Guangxi University of Science and Technology, Liuzhou 545006,

China (e-mail: chuanlin@gxust.edu.cn; yijuncaoo@gmail.com). Corresponding author: Chuan Lin.

Yong-Jie Li is with the School of Life Science and Technology, University of Electronic Science and Technology of China, Chengdu 610054, China (email: lijy@uestc.edu.cn).

To solve this challenging problem of learning a crisp edge detector using CNNs, Wang et al. [11] proposed a CED model with backward-refining decoding part fusing the feature map with intermediate features along the forward-propagating encoding part. With the help of sub-pixel convolution [14] for upsampling, CED significantly makes the boundaries crisp. Starting from the loss function, Deng et al. [15] introduced a novel loss with fusing weighted cross-entropy and dice coefficient for boundary detection.

Inspired by the backward-refining decoding architecture, we propose a novel deep refinement network (DRNet) which expands previous refinement architecture in a hierarchical manner that deepens the refinement network to extract detailed features. Specifically, some refinement modules explicitly exploit information available along the side outputs of the encoding process, and the other refinement modules try to refine the output features. In addition, considering the multi-annotation problem in the contour detection task, such as in a BSDS500 dataset including 5–10 annotations per image, we simply revised the original weight cross-entropy and dice coefficient to make full use of the label’s information. Finally, the two losses are weighted adaptively to observe which one performs better and has less hyperparameters compared with setting weights manually.

Beyond the same goal of crisp boundary detection, different studies differently evaluate crispness with a boundary map. Wang et al. [11], followed the evaluation method proposed in [16], take a tighter matching distance, while Deng et al. [15] consider that directly evaluating the boundary maps without standard non-maximal suppression (NMS) is simpler yet effective for the same purpose.

However, the above-mentioned two methods are different. If a pixel is detected on a small tolerance, it is not necessarily detected on a large tolerance, e.g. the red and blue pixels in Fig. 1(e). Furthermore, if a pixel is true positive on the original HED output, the pixel is not necessarily detected on the map after postprocessing, e.g. purple pixels in Fig. 1(e), where the purple pixels indicate $D_{GT} \cap E_a \cap E_b$ and D indicates the background union. The evaluation method with a strict matching distance mainly focuses on finding higher localized edges, called localness, while the other looks at purely evaluating the model output without any other process, called thickness. Thus, in this paper, we use the localness and thickness to evaluate the crisp boundary.

In most cases, the improvement of one means a decrease in the performance of the other. This gives us a new challenge: how to synchronously improve localness and thickness. Previous studies try to solve this in two ways: CNN architecture, e.g., CED [11] and loss function, such as that discussed in Ref. [15]. However, they tend to solve one aspect rather than improving localness and thickness simultaneously. For improving localness and thickness as much as possible, we propose a novel deep refinement network (DRNet) and loss function achieving state-of-the-art performance. Detailed ablation experiments are performed to show the impact of each component on localness and thickness boundaries. Our contributions are summarized into three parts.

1. We propose a novel network DRNet comprising multiple layers, and each layer contains multiple refinement modules. The DRNet can integrate hierarchical features

and improve localness performances.

2. We propose an effective loss function involving two parts: improved cross-entropy and Dice coefficient. We then combine them adaptively to automatically update the weights for convergence into balance. The proposed loss is a simple extension to multi-loss fusion and improves performance.
3. Ablation experiments are conducted to determine which component helps to improve crisp boundary detection. Furthermore, our experiments show that our method outperforms previous state-of-the-art methods on the BSDS500 and NYUDv2 datasets.

The remainder of this paper is organized as follows. Section 2 presents related work. Section 3 describes our CNN architecture and loss function. In Section 4, we evaluate localness and thickness edges, make a detailed ablation study, show the affection of each component, and compare our method to current state-of-the-art boundary detection methods. Finally, in Section 5, we discuss our work and possible future directions.

2 RELATED WORKS

Early contour detection approaches were focused on finding local discontinuities, normally brightness, in image features. Prewitt [17] operators detect edges by convolving a grayscale image with local derivative filters. Marr and Hildreth [18] used zero crossings of the Laplacian of Gaussian operator to detect edges. The Canny detector [19] also computes the gradient magnitude in the brightness channel, adding postprocessing steps, including non-maximum suppression and hysteresis thresholding.

More recent approaches employ multiple image features such as color and texture information and use biologically motivated methods [20–22] or learning techniques [23–29]. Martin *et al.* [23] built a statistical framework for difference of brightness (BG), color (CG), and texture (TG) channels and used these local cues as inputs for a logistic regression classifier to predict the probability of boundary (Pb). For integrating multiple scales of information, Ren *et al.* [25] utilized local boundary cues, including contrast, localization, and relative contrast. To fully utilize global visual information, Arbelaez *et al.* [12] proposed a global Pb (gPb) algorithm that extracted contours from global information by using normalized cuts to combine the above-mentioned local cues into a globalization framework. Ren *et al.* [26] used sparse code gradients (SCG) to extract salient contours from sparse codes in oriented local neighborhoods. Lim *et al.* [27] proposed a fast and accurate edge detector for both learning and detecting local contour-based representations of mid-level features called sketch tokens. Khoreva *et al.* [30] introduced the problem of weakly supervised object specific boundary detection and suggested that good performance can be obtained on many datasets using only weak supervision (*i.e.*, leveraging bounding box detection annotations without the need for instance-wise object boundary annotations). Dollar *et al.* [31] employed random decision forests to represent the structure presented in local image patches. By inputting color and gradient features, the structured

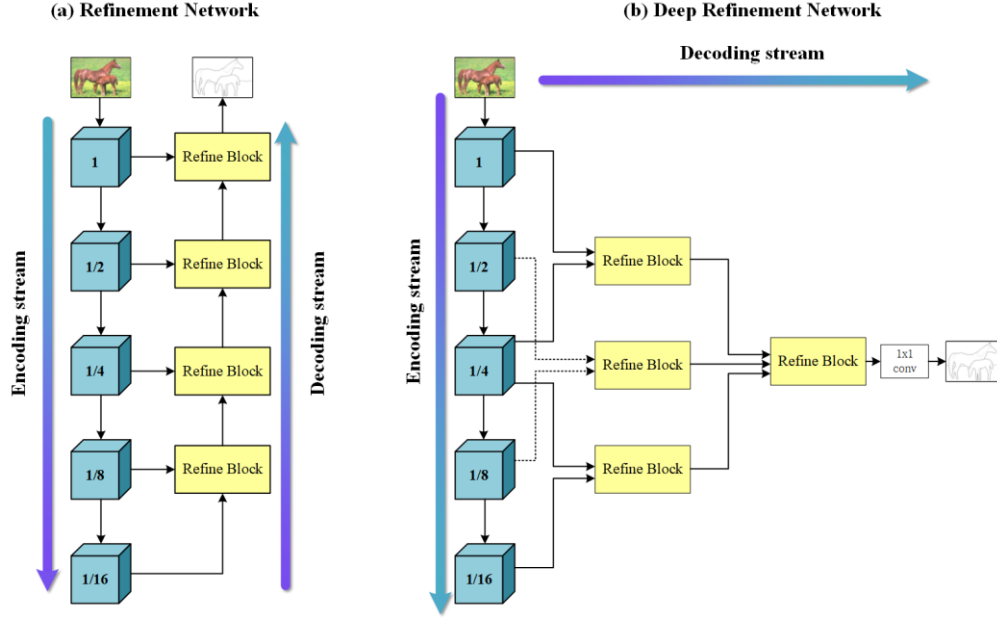


Fig. 2. Comparison of our DRNet and a previous refinement network. (a) Common refinement architectures. (b) DRNet.

forests output high-quality edges. However, all these methods are developed based on handcrafted features, which are limited in terms of their ability to represent high-level information for semantically meaningful edge detection.

In recent years, convolutional neural networks (CNNs) have been widely used in computer vision and machine learning. Ganin *et al.* [32] proposed N⁴-Fields that use a deep architecture to extract features of image patches. They approached contour detection as a multiclass classification task by matching the extracted features to predefined ground-truth features. Bertasius *et al.* [33] made use of features generated by pretrained CNNs to regress and classify the contours. They proved that object-level information provides powerful cues for the contour prediction. Shen *et al.* [8] learned deep features using mid-level information. The above-mentioned methods only used CNNs as a local feature extractor and classifier rather than using global image information to build end-to-end training. Inspired by FCN [19], Xie and Tu [9] developed an end-to-end CNN to boost the efficiency and accuracy of contour detection, called HED, using convolutional feature maps and a novel loss function. HED connects its side output layers, which is composed of one *conv* layer with kernel size 1, one *deconv* layer and one softmax layer, to the last *conv* layer of each stage in the VGG16 network. Based on the HED architecture, Kokkinos [34] built multi-scale HED and improved the results by tuning the loss function and adding globalization. Liu *et al.* [10] added the side output layers upon HED to extract richer convolutional features. In addition, Yang *et al.* [35] proposed an encoder-decoder architecture to tackle the contour detection task. Maninis *et al.* [36] proposed modeling the orientation of edges. However, these results tend to emphasis on the “correctness” of edges by selecting an optimistic matching distance and overlook the “crispness” of edges.

To improve the “crispness” of edges further, Wang *et al.* [11] combined the refinement scheme with sub-pixel convolution [14] into a novel architecture that was specifically designed for learning crisp edge detection. Deng *et al.* [15] introduced a

novel loss for boundary detection, which is very effective for classifying imbalanced data, and it allows CNNs to produce crisp boundaries.

Our method is motivated by Wang *et al.* [11] and Deng *et al.* [15]. Both proposed an end-to-end bottom-up/top-down architecture for learning crisp boundaries, and Deng *et al.* [15] introduced the dice coefficient to obtain thick edges. We share the same goal of designing a crisp edge detector, yet our method further improves the performance. Finally, our method is inspired by Kendall *et al.* [37], wherein they proposed a group of learnable weight variables for multi-task learning.

3 PROPOSED METHOD

In this section, we describe the details of the proposed method. We first describe the proposed DRNet and each component used in building this architecture. We then present adaptive weight loss by fusing the improved cross-entropy and dice loss.

3.1 Network architecture

Generic refinement architecture, such as that used in Refs. [11] and [15], includes a top-down encode network, similar to the instance on the left side of Fig. 2(a), and a down-top decode network that aims at fusing multi-resolution side outputs of encode parts. Previous studies have shown that this architecture excels at capturing hierarchical features and is able to fuse them at different stages so as to generate semantically meaningful contours. The reason of making the structure effective is to make features with different resolutions blendable. Inspired by this idea, we proposed a novel refinement network DRNet, as shown in Fig. 2(b), that horizontally expands the depth of the network to extract richer and more complex feature maps with the aim of improving the generalization ability of the model.

The core of DRNet involves remix refinement modules. We aim to exploit the integration of multi-level features for high-resolution prediction in end-to-end computer vision tasks.

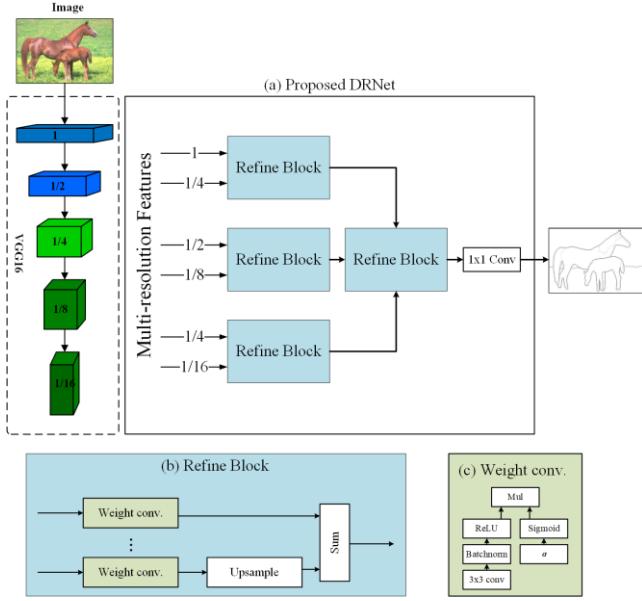


Fig. 3. Detailed DRNet architecture. (a) DRNet fusing multi-resolution features. (b) Refine block in our architectures. (c) Proposed weight convolution layer.

Compared to a traditional refinement network that combines intermediate features along the forward-propagating pathway, DRNet fuses the refinement outputs and thus makes the network learning features more accurate.

We use the VGG-16 model as the backbone and stack its ‘refactored’ structure of the refinement module to recover the resolution of features. The detailed architecture is shown in Fig. 3. We have the following development at the network to make it suitable for edge detection.

Connections. Two types of connection methods exist in the refine blocks: skip and adjacent connections. The former receives feature maps with four-time resolution difference. For example, Fig. 3(a) the right module receives (1, 1/4), (1/2, 1/8) and (1/4, 1/16) size feature maps as input and then upsamples the lower one for fusion. The adjacent connection receives three adjacent inputs, as shown in Fig. 3(a), as the right refine block. The block fuses the different resolution map by upsampling every low-resolution part to the highest one.

Refine block. Fig. 3(b) shows the detailed refine block in the proposed architecture. The refinement module includes upsample, point-wise sum, and weight convolution layers. Owing to the feature maps of each stage of VGG16 having different resolutions, we utilize bilinear upsampling to upsample the low-resolution feature maps into a high-resolution one. In addition, we use an element-wise add layer to fuse multiple inputs rather than a 1×1 convolution layer after concatenating multiple inputs because the element-wise add layer is a trade-off between performance and the number of training parameters. The output channel is set to the small one in the same refine block. After the last refine block, a 1×1 convolution layer will compress the features into one channel.

Weight convolution. Different resolutions will affect feature proportion of the final output boundary. Thus, we design a weight convolution block for automatically balancing each feature. As shown in Fig. 3(c), the weight convolution layer includes two streams, one involving a normal 3×3 convolution following batch norm and ReLU layer, and another involving a

sigmoid function—activated trainable parameter α . The feature map obtained by the first stream is automatically weighted by the second one. In our experiment, the weight convolution layer should improve the performances compared with the traditional convolution layer and has less computational cost.

Our network is simple yet very effective for edge detection. During the forward pass, these refine blocks of first level convey and decode the multi-resolution features and then transmit them into separate refine blocks for further refining. Compared to the original structure, our network has the advantage of using similar parameters to achieve better performance.

3.2 Adaptive weigh loss for boundary detection

Loss function is the most important component in end-to-end CNNs as the quality of prediction is most affected by its loss. On the CNN-based boundaries detection task, loss design generally accounts for 1) positive and negative sample trade-off; 2) application of multi-annotation information in binary classification; 3) multiple losses combination; and 4) contour performance development. Aiming at the last three points, we first revisit the weighted cross-entropy and the dice coefficient (Section 3.2.1) loss for making full use of multi-annotation information, thereby improving performance. Then, considering the balance of cross-entropy and dice loss, we propose a novel method to combine these losses without hand-specific weights and obtain good performance.

3.2.1 Improved cross-entropy and dice coefficient loss

We start by looking into the weight cross-entropy proposed in HED[9]. It is well known that the cross-entropy loss is used to solve binary classification. However, the edge/non-edge pixels have a highly imbalanced distribution (the majority of pixels are non-edge); thus, the direct use of cross-entropy loss would fail to train the network. To tackle the issue, HED uses weighted cross-entropy loss, which writes

$$CE(P, L) = -\beta \sum_{i \in L_+} \log p_i - (1 - \beta) \sum_{i \in L_-} \log(1 - p_i) \quad (1)$$

where L_+ and L_- denote the edge pixel set and non-edge pixel sets, respectively. $\beta = |L_-|/|L|$ and $1 - \beta = |L_+|/|L|$. p_i is the CNN output processed by sigmoid function at pixel i . By using weights β and $1 - \beta$, this solution help CNNs better train the network.

As for the multiple annotator problem, HED adopts a relatively brute-force solution: it only assigns a positive label to a pixel if it is labeled as positive by at least three annotators; it regards all other labeled pixels as negatives. Subsequently, RCF [10] considers the pixels as positive samples only if it is labeled by higher than 50% annotators and pixels without any positive label are treated as negative samples. Otherwise, if a pixel is marked by fewer than 50% of the annotators, this pixel is ignored during training (by blocking their gradients).

However, the above-mentioned methods seem a bit too aggressive. Though these human-labeled edge maps (5–10) share a little consistency, more potential information might be discarded. Thus, we convert the problem of judging the positive and negative samples into the problem of weighting. Thus, we first transform multiple annotation averaging to a weight map:

$$W = \frac{1}{n} \sum_{i=1}^n L^i \quad (2)$$

where n is the number of annotators for each image and L^i indicates the i -th annotate map. W is the probability label map by averaging all ground truth, which ranges from 0 to 1. We consider a pixel a positive label if $W > 0$, which means if it is labeled as positive by at least one annotator.

Then, each positive labeled pixel is weighted using W . The new loss is named as soft cross-entropy (SCE) and is written as follows.

$$\text{SCE}(P, W) = -\frac{\beta}{|Y_+|} \sum_{i \in \{W>0\}} W_i * \log p_i - \frac{(1-\beta)}{|Y_-|} \sum_{i \in \{W=0\}} \log(1 - p_i) \quad (3)$$

where $\{W > 0\}$ denotes the positive label set where $W > 0$, and $\{W = 0\}$ is the non-edge pixel set where $W = 0$. Each positive pixel weight using a probability label map W at pixel i . We also normalized, respectively, positive and negative loss to avoid the imbalance range of the value with the adaptive weighting method (Section 4.2.2). Compared with (1), the proposed loss is simple yet very effective for edge detection.

A distinct characteristic of edge map has highly biased data because the vast majority of the pixels are non-edges. This phenomenon would cause learning to fail at finding the crisp edges. For this issue, Deng et al. [15] introduced dice coefficient loss for learning crisp boundaries, which is as follows

$$D(P, L) = \frac{\sum_i^N p_i^2 + \sum_i^N l_i^2}{2 \sum_i^N p_i l_i} \quad (4)$$

where p_i and l_i denote the i -th pixel on the prediction map P and the label L , respectively. N denotes the total number of input images. However, this loss does not consider the multiple annotation issues as well. Thus, we simply revised it to suit different label maps and named soft dice loss (SD) as follow.

$$\text{SD}(P, W) = \frac{\sum_i^N p_i^2 + \sum_i^N W_i^2 + \varepsilon}{2 \sum_i^N p_i W_i + \varepsilon} \quad (5)$$

where we simply substitute ground truth map L to probability label map W . ε is introduced for avoiding the loss to Nan and is set to a value of $1e-6$.

3.2.2 Adaptive fusion

To achieve a better performance, the SCE and SD can be combined as one loss function, which is given by

$$L(P, W) = \kappa \text{SCE}(P, W) + \tau \text{SD}(P, W), \quad (6)$$

where $\text{SCE}(P, W)$ is the improved cross-entropy loss, defined as Equation 3; $\text{SD}(P, W)$ is the improved Dice loss, defined as Equation 5; and κ and τ are the parameters that control the influence of the two losses.

However, the uncertain parameters κ and τ control the relative confidence between the losses. Although we can assign them by hand, it is difficult to obtain the optimal balance point to enhance performance. Inspired by a previous study [37], which proposed the homoscedastic uncertainty as a basis for the weighting losses in a multi-task learning problem, we modified the proposed theory for fusion multiply losses in a boundary detection task problem. Specifically, the final adaptive weight loss (AWL) function is defined as

$$L_{final}(P, W) = \frac{1}{\kappa^2} \text{SCE}(P, W) + \frac{0.1}{\tau^2} \text{SD}(P, W) + \log(1 + \kappa\tau) \quad (7)$$

The auxiliary term, $\log(1 + \kappa\tau)$ can be regarded as a weight learning term. Large values of κ and τ decrease the contribution of the loss term $\frac{1}{\kappa^2} \text{SCE}(P, W) + \frac{0.1}{\tau^2} \text{SD}(P, W)$, whereas small values of κ and τ increase its contribution. The parameters κ and τ are regulated by the last term. During training, both terms mutually interact with and restrict each other, and thus, can automatically balance each other. More importantly, this type of method has good extendibility, which means that we can simply revise Eq. (7) to combine three or more loss terms.

In practice, we set the auxiliary term as $\log(1 + \kappa\tau)$ rather than $\log(\kappa\tau)$ due to its numerical stability. A fixed value of 0.1 is used to ensure that the output range of the different loss functions is within the order of magnitude.

3.3 Multi-scale contour detection

We construct image pyramids to detect multi-scale contours, as used in previous studies [10, 11]. Specifically, we resize an image to construct an image pyramid, and each of these images are separately input to our DRNet. Then, all the resulting edge probability maps are resized to the original image size using bilinear interpolation. Finally, these maps are averaged to obtain a final prediction map. Considering the trade-off between accuracy and speed, we use three scales, namely, 0.5, 1.0, and 2.0, in this study.

4 EXPERIMENTS

4.1 Implementation details

Hyperparameters. We implemented our network using the publicly available PyTorch [38], which is well-known in this community. The backbone VGG16 was pretrained on ImageNet [39]. For training, the hyperparameters of our model included: mini-batch size (10), global learning rate (0.01), learning rate decay (0.1) after five training epochs, weight decay ($1e-4$), and input image resolution (320×320). SGD was used and the momentum was set to 0.9. The total number of training epochs was 30. The trainable parameters κ and τ were both set to 1.

Data augmentation. Data augmentation is an effective way to boost performance when the amount of training data is limited. First, we randomly scaled the image-label pairs (0.75–1.25). Then, on the BSDS500 dataset, we rotated the pairs in 16 different angles and flipped the image at each angle. Finally, we flipped the cropped images, which resulted in an augmented training set from 200 images to more than 100 K images. On the NYUD-v2 dataset, we rotated the images and corresponding annotations in four different angles (0, 90, 180, and 270°) and flipped them at each angle.

Dataset. We used BSDS500 [12] and NYUD [13] for our experiments. BSDS500 [12] is a widely used dataset in edge detection. It is composed of 200 training, 100 validation, and 200 test images, and each image is labeled by multiple annotators. We utilized the training and validation sets for fine-tuning, and the test set for evaluation. Inspired by previous studies [10, 11, 34], we mixed the augmentation data of

BSDS500 with the flipped PASCAL VOC Context dataset [40] as the training data. During training, we set the loss parameter λ to 1.5 instead of 1.1 as in [10]. During evaluation, the standard non-maximum suppression (NMS) [31] was applied to thin the detected edges.

NYUD [13] dataset is composed of 1449 densely labeled pairs of aligned RGB and depth images. Recently, many studies were conducted on the edge evaluation on this dataset [10, 26, 31]. Gupta et al. [41] split the NYUD dataset into 381 training, 414 validation, and 654 test images. We followed their settings and trained our network using the training and validation sets in full resolution as in HED [9]. We utilized the depth information by using HHA [42], in which the depth information is encoded into three channels: horizontal disparity, height above the ground, and angle with gravity. Thus, the HHA features can be represented as a color image. Then, two models for the RGB images and HHA feature images were trained separately. We rotated the images and corresponding annotations to four different angles (0, 90, 180, and 270°) and flipped them at each angle. For the training process, the network settings were the same as those used for BSDS500. During testing, the final edge predictions were defined by averaging the outputs of the RGB model and HHA model. During evaluation, we increased the localization tolerance, from $maxDist = 0.0075$ to 0.011, which is the same as that in [10], because the images in NYUD dataset are larger than those in BSDS500 dataset.

4.2 Evaluation of crisp boundaries

As per previous studies [11, 15], good boundary detections must be both “correct” (detects real object boundaries) and “crisp” (precisely localized along the object’s contour). Additionally, directly learning a thick boundary without any other post-processes is an important ability in modern CNNs as well. However, the standard evaluation benchmark [23] does not distinguish between these criteria. According to previous work, we use three criteria to evaluate correct and crisp boundaries.

The first criterion is the standard evaluation benchmark evaluating boundaries [23], which test the output images with a tolerance of $d_0 = 4.3$ pixels (corresponding to the parameter $maxDist = 0.0075$ for BSDS500) after standard post-processes (NMS and morphological thinning). This default setting can evaluate the correctness of the boundaries; however, it cannot distinguish whether or not an algorithm captures the details of the edges. For evaluating the localness of the edges, we decreased the tolerance to $d = d_0/4$ and used standard post-processes for testing the localness contours, as in [11, 15]. The thickness of the edges was measured with the default tolerance d without standard post-processes, as in [23].

The prediction accuracy was evaluated via three standard measures: fixed contour threshold (ODS), per-image best threshold (OIS), and average precision (AP). In the ablation study, we only used the ODS to verify the three criteria, correctness, localness, and thickness, because the trends of ODS, OIS, and AP are similar. For conciseness, we use the notations, ODS-C, ODS-L, and ODS-T, to indicate ODS for correctness, localness, and thickness, respectively.

4.3 Ablation study

Per-image and per-batch training. First, we tested the performance using per-image and per-batch training. In this experiment, we used the SCE loss for training. From Table 1, we can observe that using the per-image average to compute the loss function is a better choice. Owing to this, we exploit the per-image training for the following experiments.

Table 1. Ablation study for per-image and per-batch training.

	ODS-C	ODS-L	ODS-T
Per-image	0.800	0.595	0.662
Per-batch	0.782	0.575	0.658

Network architecture. To evaluate the performance of the proposed method (named deep refinement contour, DRC), we conducted experiments with several settings, including using the original DRC as our baseline, training different versions of DRC with and without batch norm, and weight convolution. Table 2 shows that the proposed weight convolution layer outperforms the original convolution with a batch normalized layer, as weight convolution can adaptively balance features of different resolutions through weighing coefficient learning. Moreover, the batch norm layer is abandoned in most previous works, such as those on HED [9] and RCF [10], while a better ODS was obtained in our experiments. These results can be rationalized as follows. We know that the batch norm layer can improve generalization (reduce overfitting). However, the traditional brute-force solution only uses absolutely credible labels for training, and thus, needs some overfitting to ensure the integrity of the contour. In summary, the weight convolution can improve the performance. Additionally, when SCE is used, the batch norm can improve the performance, whereas when the loss in HED [9] and RCF [10] is used, the batch norm may decrease the performance.

Table 2. Ablation studies of the network architecture.

Method	BN	W. Conv.	ODS-S	ODS-L	ODS-T
DRC	×	×	0.789	0.589	0.647
	✓	×	0.796	0.590	0.656
	✓	✓	0.800	0.595	0.662

Loss function. First, we tested the performance of SCE and SD. Table 3 shows that the proposed SCE loss outperformed the original version because of the use of traditional loss. Furthermore, we combined the SD loss directly, as in Eq. (6). A general tendency demonstrates that fusing SCE and SD aids in improving the ODS-L and ODS-T performances, whereas independently adapting the SD loss to train the network leads to poor results. Fig. 4 illustrates contour maps using different loss combinations without any postprocessing. We can observe that the proposed SCE loss is able to obtain more details and increase the crispness of the contour; on the other hand, the use of SD loss for training allows one to obtain better edge thickness at the price of losing many useful details. We evaluated the AWL in comparison with the hand-specified weight. Table 4 presents the models trained on different weight combinations. We can observe that the joint loss performed better than the individual losses, and the weight combination ($\kappa = 1.5, \tau = 0.5$) outperformed the others on ODS-S and

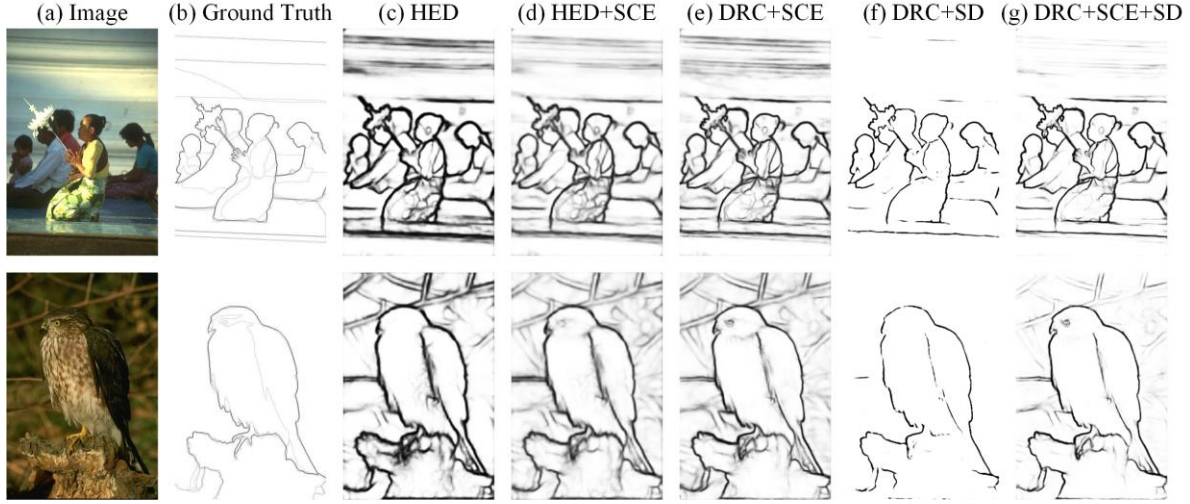


Fig. 4. Illustration of the qualitative results of the ablation study. (a) input images in the BSDS500 dataset; (b) ground truth; (c) and (d) are the predictions of HED and HED with proposed SCE loss, respectively; (e), (f) and (g) are the predictions of the proposed methods DRC with SCE, SD, and SCE+SD loss in the comparative study, respectively.

ODS-L measurements, whereas ($\kappa = 1.0, \tau = 1.0$) exhibited good ODS-T performance. However, determining these optimal weightings is expensive and increasingly difficult for large models with numerous losses. The last row in Table 4 indicates the quantitative result of the proposed AWL, and the performances are better than the other hand-specified weights. Although the increase is not large, the role of AWL will become more apparent as more cost functions are combined.

Table 3. Ablation studies of the loss function.

Method	SCE	SD	ODS-S	ODS-L	ODS-T
HED	×	×	0.780	0.548	0.583
	✓	×	0.795	0.560	0.613
DRC	×	×	0.796	0.581	0.633
	✓	×	0.800	0.595	0.662
	×	✓	0.725	0.551	0.656
	✓	✓	0.798	0.601	0.683

Table 4. Comparison of loss weightings between hand-specified and proposed AWL method.

Loss Weights		Performances		
κ	τ	ODS-S	ODS-L	ODS-T
0	1	0.725	0.551	0.656
0.25	1.75	0.786	0.593	0.666
0.5	1.5	0.792	0.597	0.666
0.75	1.25	0.796	0.600	0.672
1	1	0.798	0.601	0.683
1.25	0.75	0.801	0.601	0.671
1.5	0.5	0.802	0.602	0.671
1.75	0.25	0.801	0.600	0.673
1	0	0.800	0.595	0.662
Learned weights		0.802	0.605	0.687

Multi-scale and more training data. As can be observed from Table 5, in comparison with the single-scale version, the multi-scale DRC (DRC-MS) surprisingly has the worst performance. This is because the SCE loss contains potential multi-scale information. After simply augmenting the standard BSDS500 training dataset with the VOC images as in previous studies [9-11, 15], the multi-scale DRC (DRC-MS-VOC) exhibits better results with ODS-S and ODS-L, and worse results with ODS-T. Therefore, to improve the correctness and localness performances, one needs to use additional VOC

images for training and compute the contour map by using the multi-scale method. On the other hand, to obtain better thickness of the edges without any postprocessing, the original DRC should be used.

Table 5. Ablation studies of the multi-scale version and PASCAL VOC for mix training.

Method	MS	VOC	ODS-S	ODS-L	ODS-T
DRC	×	×	0.802	0.605	0.687
	✓	×	0.798	0.596	0.684
	×	✓	0.806	0.586	0.664
	✓	✓	0.818	0.623	0.670

Efficiency analysis. Contour detection, as a preprocessing step toward high-level applications, needs to be computationally efficient. In our experiments, the single-scale version achieved a value of 30 FPS (0.041 s) when processing a 481×321 resolution image on a GTX 1080Ti GPU. Because our method is simple, effective, and extremely fast, it is easy to be used in high-level vision tasks, such as image segmentation. The multi-scale version is relatively slower, with a value of approximately 5.5 FPS (0.182 s) with the same settings.

4.4 Comparison with state-of-the-art methods

BSDS500. We compared our method with several non-deep-learning algorithms, such as Canny [19], gPb-UCM [12], and SE [31], and recent deep learning based approaches, such as DeepContour [8], DeepEdge [33], HED [9], CED [11], COB [36], and RCF-MS [10]. Fig. 5 depicts the Precision-Recall curves, and Table 6 presents the evaluation results in terms of standard ODS, OIS, and AP. Our DRC achieved better results than the top-performing method in ODS and OIS. This result also surpassed the human benchmark on the BSDS500 dataset with ODS (0.803). The RCF-MS [10], CED [11], and TB [15] mixed PASCAL VOC Context into BSDS500, whereas the other methods only used the BSDS training set. The best performance was exhibited by CED [11]. This method achieves better AP performance, as it uses HED pretrained models, apart from ImageNet, on the VGG16 backbone.

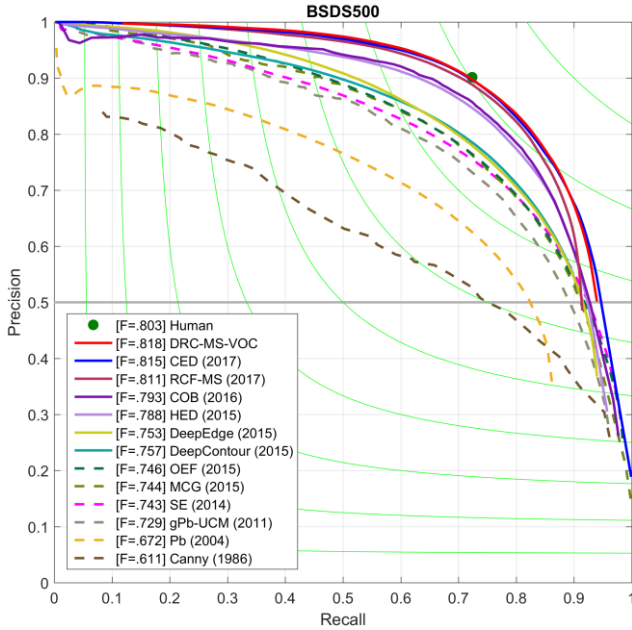


Fig. 5. Precision-recall curves of BSDS500.

Table 6. Quantitative comparison on BSDS500 dataset.

Method	ODS	OIS	AP
Canny [19]	0.611	0.676	0.520
gPb [12]	0.729	0.755	0.745
SE [31]	0.743	0.764	0.800
DeepContour [8]	0.757	0.776	0.790
DeepEdge [33]	0.753	0.772	0.787
HED [9]	0.788	0.808	0.840
COB [36]	0.793	0.819	0.849
RCF-MS [10]	0.811	0.830	0.846
CED [11]	0.816	0.833	0.889
TB [15]	0.815	0.834	-
DRC	0.802	0.818	0.800
DRC-MS-VOC	0.818	0.836	0.757

Table 7. Comparison of crispness of edges on BSDS500 dataset.

Method	ODS-L	OIS-L	ODS-T	OIS-T
Human	0.625	-	-	-
HED [9]	0.551	0.561	0.585	0.599
CED [11]	0.609	0.619	0.655	0.662
TB [15]	-	-	0.693	0.700
DRC	0.605	0.614	0.687	0.696
DRC-MS-VOC	0.623	0.635	0.670	0.680

We further benchmarked the crispness of edges. We compared our method with the state-of-the-art HED, CED, and method proposed in [15] (named thick boundary, TB). The results are summarized in Table 7. Our models (DRC-MS-VOC) outperformed the state-of-the-art HED and CED, and achieved $ODS-L=0.623$ at $d_0/4$, which is close to the human level performance ($ODS-L=0.625$). In addition, the proposed single-scale version of DRC achieved $ODS-T=0.687$. This value is slightly less than that of TB ($ODS-T=0.693$) because this method uses the *ResNeXt* block, which aids in improving the thickness performance.

NYUD. Fig. 6 illustrates an overview of the data with the HHA features that we used, as well as the results obtained by DRC. We trained the CNNs on three versions: using only RGB data (DRC-RGB), (b) using only HHA data (DRC-HHA), and

(c) directly adding RGB and HHA output (DRC-RGB-HHA). We observe that the RGB-HHA version obtained significantly better results in standard correctness than the one trained on RGB or HHA data.

Table 8. Quantitative comparison on NYUD-V2 dataset.

Method	ODS	OIS	AP
gPb-UCM [12]	0.631	0.661	0.562
SE [31]	0.695	0.708	0.719
gPb+NG [41]	0.687	0.716	0.629
SE+NG+ [42]	0.706	0.734	0.549
HED [9]	0.741	0.757	0.749
RCF [10]	0.757	0.771	0.749
TB [15]	0.762	0.778	-
COB [36]	0.784	0.805	0.825
COB-original [36]	0.745	0.762	0.792
DRC-RGB	0.741	0.755	0.741
DRC-HHA	0.699	0.712	0.694
DRC-HHA-RGB	0.763	0.775	0.776

We compared our method with several non-deep-learning algorithms, such as gPb-UCM [12], SE [31], gPb+NG [41], SE+NG+ [42] and recent deep learning based approaches, such as HED [9], COB [36], and RCF [10]. The Precision-Recall curves are depicted in Fig. 7, and the quantitative comparison is presented in Table 8. The best result was exhibited on NYUD by COB [36], where the authors used the more powerful UCM [12] algorithm in post-processes, which is more advantageous for contour performance. We named the version without UCM as COB-original. The proposed DRC was higher than COB-original in standard measurements.

We further reported the “crispness” of the edges of the proposed DRC. In the NYUD dataset, the default setting of $maxDist=0.011$ was used rather than 0.0075 in BSDS. Thus, we set $maxDist=0.011/4=0.00275$ for the ODS-L measurement. Table 9 presents the experimental results. The contour accuracy was poor for complex and meticulous scenes of high resolution. In contrast to the BSDS500 dataset, NYUD-v2 includes high-resolution images, which contain more complex coarse and fine contours. Although DRC obtained a good “crispness” boundary on BSDS500, our results were not quite satisfactory for more complex databases, such as NYUD-v2. We also observed that in a stricter comparison, such as that of ODS-L with ODS-T, merging the HHA and RGB data could not achieve better performances, as can be observed in Table 9. Especially for the ODS-T measurement, the HHA-RGB version was worse than the single RGB version.

Table 9. Crispness of edges on NYUD-V2 dataset.

Method	ODS-L	OIS-L	ODS-T	OIS-T
DRC-HHA	0.282	0.410	0.288	0.421
DRC-RGB	0.358	0.477	0.365	0.489
DRC-HHA-RGB	0.358	0.429	0.366	0.439

5 DISCUSSION AND CONCLUSION

We demonstrated that the crispness boundary performances can be evaluated in two ways: localness [11, 16], and thickness [15]. For improving these two performances, we proposed a novel method for the challenging tasks. The main novelty of proposed model is summarized as follows. (a) A new CNN architecture, called DRNet, was employed. Although the

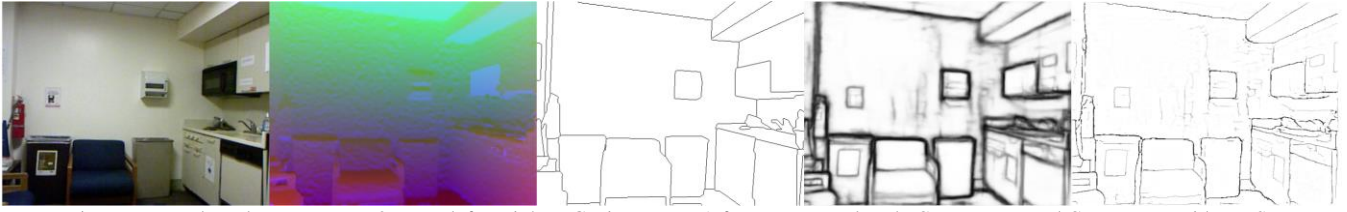


Fig. 6. Data and results on NYUD-v2. From left to right: RGB image, HHA features, ground truth, CNN output, and CNN output with NMS.

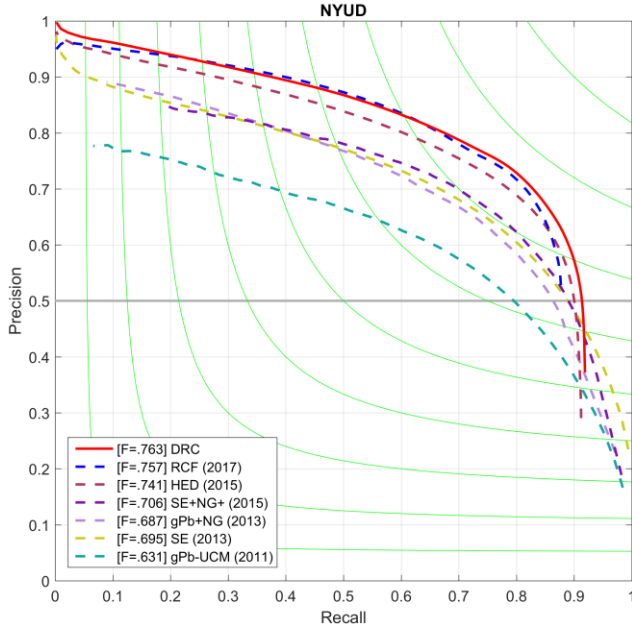


Fig. 7. Precision-recall curves of NYUD-V2.

network appears simple, it includes an interesting idea of decoding feature remixing. Based on this, we can easily design a more complex network for several tasks. In addition, the DRNet involves a useful component, namely the weight convolution layer (see Section 3.1), which can automatically learn the feature weights in end-to-end learning. The experiments demonstrated that this layer improves performance for the three benchmark evaluations (see Table 2). (b) We improved a novel loss function, known as the multi-loss combination framework. In this framework, we could easily fuse multiply losses, which often exhibit different distinguishing features, training them without manually assigning the weights. Another contribution is the addition of a multi-label version of the traditional loss, such as cross-entropy and Dice coefficient. These new versions aim at making full use of each annotation information and the experiments (see Table 3) demonstrate their advantages.

The quantitative results on the two benchmark datasets (i.e., BSDS and NYUD-V2) and three measurements (correctness, localness, and thickness) demonstrate that the DRC systematically improves the state-of-the-art in most comparisons. In the standard correctness comparison, we achieved a new state-of-the-art in BSDS500 (ODS=0.818) and NYUD-V2 (ODS=0.763) when using the standard post-processes (NMS and morphological thinning). More importantly, we significantly improved the localness performance by 2.3%, achieving ODS=0.623, which is close to that of the human level (ODS=0.625). However, the thickness performance did not achieve state-of-the-art. This also implies

that it is more difficult to increase both localness and thickness than to increase the two individually. In the NYUD-V2 comparison, the DRC outperformed most of the methods on correctness performances, except the COB [36] with the UCM algorithm. The crispness results (see Table 9) have shown that in high-resolution image datasets and more rigorous evaluation criteria, the existing contour detection algorithms still have a considerable scope for improvement.

A more challenging task is to determine a method that performs well in both correctness and crispness. The experiments (see Table 1–5 in Section 4.2) demonstrated that the loss function, training methods, components of CNNs, etc., may influence the final performances. The most obvious method to have an influence is the multi-scale and VOC hybrid training method. If we only use the multi-scale algorithm, all three performances will decrease (under the SCE training). When we used the multi-scale and mixing VOC for training, the performances of ODS-S and ODS-L significantly improved and that of ODS-T decreased. Hence, algorithms excellent in one respect should not be selected at all times. Instead, one should choose methods that perform well in both correctness and crispness evaluation as standard components for CNN design.

In this study, we analyzed the evaluation criteria for crisp boundaries and proposed a novel method that focuses on crisp contour detection. Specifically, we proposed a novel CNN architecture, DRNet, that makes use of the multi-level refinement modules to build deep networks, and a new approach that can combine the multiply losses and automatically learn the weights of the different loss functions. Detailed ablation studies and comparisons suggest that the high-quality contour detector achieved promising performance on BSDS500 and NYUD-v2. We hope that the proposed methods can inspire subsequent research on contour detection, and further aid in improving other visual tasks.

REFERENCES

- [1] L. Liang, M. Wei, A. Szymczak, W.-M. Pang, and M. J. I. T. o. M. Wang, "Spin contour," *IEEE Transactions on Multimedia*, vol. 18, no. 11, pp. 2282-2292, 2016.
- [2] Y. Zhang, X. Qian, X. Tan, J. Han, and Y. Tang, "Sketch-based image retrieval by salient contour reinforcement," *IEEE Transactions on Multimedia*, vol. 18, no. 8, pp. 1604-1615, 2016.
- [3] S. Wang, J. Zhang, T. X. Han, and Z. J. I. T. o. M. Miao, "Sketch-based image retrieval through hypothesis-driven object boundary selection with HLR descriptor," *IEEE Transactions on Multimedia*, vol. 17, no. 7, pp. 1045-1057, 2015.
- [4] A. Krizhevsky, I. Sutskever, and G. E. Hinton, "Imagenet classification with deep convolutional neural networks," in *Advances in Neural Information Processing Systems*, 2012, pp. 1097-1105.
- [5] K. Simonyan and A. Zisserman, "Very deep convolutional networks for large-scale image recognition," in *International Conference on Representation Learning*, 2015.
- [6] R. Girshick, "Fast r-cnn," in *International Conference on Computer Vision*, 2015, pp. 1440-1448.

- [7] X. Li, Z. Liu, P. Luo, C. C. Loy, and X. Tang, "Not all pixels are equal: difficulty-aware semantic segmentation via deep layer cascade," *IEEE Conference on Computer Vision and Pattern Recognition*, 2017.
- [8] W. Shen, X. Wang, Y. Wang, X. Bai, and Z. Zhang, "Deepcontour: A deep convolutional feature learned by positive-sharing loss for contour detection," in *IEEE Conference on Computer Vision and Pattern Recognition*, 2015, pp. 3982-3991.
- [9] S. Xie and Z. Tu, "Holistically-nested edge detection," in *International Conference on Computer Vision*, 2015, pp. 1395-1403.
- [10] Y. Liu, M.-M. Cheng, X. Hu, K. Wang, and X. Bai, "Richer convolutional features for edge detection," in *IEEE Conference on Computer Vision and Pattern Recognition*, 2017, pp. 5872-5881: IEEE.
- [11] Y. Wang, X. Zhao, and K. Huang, "Deep Crisp Boundaries," in *IEEE Conference on Computer Vision and Pattern Recognition*, 2017, pp. 3892-3900.
- [12] P. Arbelaez, M. Maire, C. Fowlkes, and J. Malik, "Contour detection and hierarchical image segmentation," *IEEE Trans. Pattern Anal. Mach. Intell.*, vol. 33, no. 5, pp. 898-916, 2011.
- [13] N. Silberman, D. Hoiem, P. Kohli, and R. Fergus, "Indoor segmentation and support inference from rgbd images," in *International Journal of Computer Vision*, 2012, pp. 746-760: Springer.
- [14] W. Shi *et al.*, "Real-time single image and video super-resolution using an efficient sub-pixel convolutional neural network," in *IEEE Conference on Computer Vision and Pattern Recognition*, 2016, pp. 1874-1883.
- [15] R. Deng, C. Shen, S. Liu, H. Wang, and X. Liu, "Learning to predict crisp boundaries," in *Proceedings of the European Conference on Computer Vision*, 2018, pp. 562-578.
- [16] P. Isola, D. Zoran, D. Krishnan, and E. H. Adelson, "Crisp boundary detection using pointwise mutual information," in *Proceedings of the European Conference on Computer Vision*, 2014, pp. 799-814: Springer.
- [17] J. M. Prewitt, "Object enhancement and extraction," *Pic. Process. and Psychopictorics*, vol. 10, no. 1, pp. 15-19, 1970.
- [18] D. Marr and E. Hildreth, "Theory of edge detection," *Proc. Roy. Soc. London B, Biol. Sci.*, vol. 207, no. 1167, pp. 187-217, 1980.
- [19] J. Canny, "A computational approach to edge detection," *IEEE Trans. Pattern Anal. Mach. Intell.*, vol. PAMI-8, no. 6, pp. 679-698, 1986.
- [20] K.-F. Yang, C.-Y. Li, and Y.-J. Li, "Multifeature-based surround inhibition improves contour detection in natural images," *IEEE Trans. Image Process.*, vol. 23, no. 12, pp. 5020-5032, 2014.
- [21] C. Lin, G. Xu, Y. Cao, C. Liang, and Y. Li, "Improved contour detection model with spatial summation properties based on nonclassical receptive field," *Journal of Electronic Imaging*, vol. 25, no. 4, pp. 043018-043018, 2016.
- [22] C. Lin, G. Xu, and Y. Cao, "Contour detection model using linear and non-linear modulation based on non-CRF suppression," *IET Image Processing*, 2018.
- [23] D. R. Martin, C. C. Fowlkes, and J. Malik, "Learning to detect natural image boundaries using local brightness, color, and texture cues," *IEEE Trans. Pattern Anal. Mach. Intell.*, vol. 26, no. 5, pp. 530-549, 2004.
- [24] P. Dollár, Z. Tu, and S. Belongie, "Supervised learning of edges and object boundaries," in *IEEE Conference on Computer Vision and Pattern Recognition*, 2006, vol. 2, pp. 1964-1971: IEEE.
- [25] X. Ren, "Multi-scale improves boundary detection in natural images," in *Proceedings of the European Conference on Computer Vision*, 2008, pp. 533-545: Springer.
- [26] R. Xiao Feng and L. Bo, "Discriminatively trained sparse code gradients for contour detection," in *Advances in Neural Information Processing Systems*, 2012, pp. 584-592.
- [27] J. J. Lim, C. L. Zitnick, and P. Dollár, "Sketch tokens: A learned mid-level representation for contour and object detection," in *IEEE Conference on Computer Vision and Pattern Recognition*, 2013, pp. 3158-3165.
- [28] Y. Li, M. Paluri, J. M. Rehg, and P. Dollár, "Unsupervised learning of edges," in *IEEE Conference on Computer Vision and Pattern Recognition*, 2016, pp. 1619-1627.
- [29] Z. Zhang, F. Xing, X. Shi, and L. Yang, "Semicontour: A semi-supervised learning approach for contour detection," in *IEEE Conference on Computer Vision and Pattern Recognition*, 2016, pp. 251-259.
- [30] A. Khoreva, R. Benenson, M. Omran, M. Hein, and B. Schiele, "Weakly supervised object boundaries," in *IEEE Conference on Computer Vision and Pattern Recognition*, 2016, pp. 183-192.
- [31] P. Dollár and C. L. Zitnick, "Fast edge detection using structured forests," *IEEE Transactions on Pattern Analysis and Machine Intelligence*, vol. 37, no. 8, pp. 1558-1570, 2015.
- [32] Y. Ganin and V. Lempitsky, "N4-fields: Neural network nearest neighbor fields for image transforms," in *Asian Conference on Computer Vision*, 2014, pp. 536-551: Springer.
- [33] G. Bertasius, J. Shi, and L. Torresani, "Deepedge: A multi-scale bifurcated deep network for top-down contour detection," in *IEEE Conference on Computer Vision and Pattern Recognition*, 2015, pp. 4380-4389.
- [34] I. Kokkinos, "Pushing the boundaries of boundary detection using deep learning," in *International Conference on Representation Learning*, 2016.
- [35] J. Yang, B. Price, S. Cohen, H. Lee, and M.-H. Yang, "Object contour detection with a fully convolutional encoder-decoder network," in *IEEE Conference on Computer Vision and Pattern Recognition*, 2016, pp. 193-202: IEEE.
- [36] K.-K. Maninis, J. Pont-Tuset, P. Arbeláez, and L. Van Gool, "Convolutional oriented boundaries," in *ECCV*, 2016, pp. 580-596: Springer.
- [37] A. Kendall, Y. Gal, and R. Cipolla, "Multi-task learning using uncertainty to weigh losses for scene geometry and semantics," in *Proceedings of the IEEE Conference on Computer Vision and Pattern Recognition*, 2018, pp. 7482-7491.
- [38] A. Paszke *et al.*, "Automatic differentiation in pytorch," 2017.
- [39] J. Deng, W. Dong, R. Socher, L.-J. Li, K. Li, and L. Fei-Fei, "Imagenet: A large-scale hierarchical image database," in *IEEE Conference on Computer Vision and Pattern Recognition*, 2009, pp. 248-255: IEEE.
- [40] R. Mottaghi *et al.*, "The role of context for object detection and semantic segmentation in the wild," in *IEEE Conference on Computer Vision and Pattern Recognition*, 2014, pp. 891-898.
- [41] S. Gupta, P. Arbelaez, and J. Malik, "Perceptual organization and recognition of indoor scenes from RGB-D images," in *IEEE Conference on Computer Vision and Pattern Recognition*, 2013, pp. 564-571: IEEE.
- [42] S. Gupta, R. Girshick, P. Arbeláez, and J. Malik, "Learning rich features from RGB-D images for object detection and segmentation," in *International Journal of Computer Vision*, 2014, pp. 345-360: Springer.